Temperature Dependent Scattering Rates at the Fermi Surface of Optimally Doped $Bi_2Sr_2CaCu_2O_{8+\delta}$

T. Valla,[1] A. V. Fedorov,[1] P. D. Johnson,[1] Q. Li,[2] G. D. Gu,[3] and N. Koshizuka[4]

[1]*Department of Physics, Brookhaven National Laboratory, Upton, New York 11973-5000*
[2]*Division of Materials Sciences, Brookhaven National Laboratory, Upton, New York 11973-5000*
[3]*School of Physics, The University of New South Wales, P.O. Box 1, Kensington, New South Wales, Australia 2033*
[4]*Superconductivity Research Laboratory, ISTEC, 10-13, Shinonome I-chrome, Koto-ku, Tokyo 135, Japan*

(Received 21 March 2000)

For optimally doped $Bi_2Sr_2CaCu_2O_{8+\delta}$, scattering rates in the normal state are found to have a linear temperature dependence over most of the Fermi surface. In the immediate vicinity of the $(\pi, 0)$ point, the scattering rates are nearly constant in the normal state, consistent with models in which scattering at this point determines the c-axis transport. In the superconducting state, the scattering rates away from the nodal direction appear to level off and become temperature independent.

PACS numbers: 74.72.Hs

Obtaining a detailed understanding of the microscopic mechanism that results in high temperature superconductivity remains one of the fundamental challenges of condensed matter physics. Angle-resolved photoemission (ARPES) has provided a number of important insights into these materials; the mapping of the Fermi surface [1], the identification of d-wave symmetry of the order parameter in the superconducting state [2], and the detection of a pseudogap for underdoped compounds above the transition temperature T_c [3,4]. Recent advances in instrumentation have allowed ARPES to be used for studies of the single-particle self-energy, Σ, a quantity that reflects fundamental interactions in a many-body system. The real part of the self-energy corresponds to the shift in energy, and the imaginary part represents the scattering rate (inverse lifetime) due to the interaction. Recently, an ARPES study has provided clear evidence that in optimally doped $Bi_2Sr_2CaCu_2O_{8+\delta}$ (Bi2212), in the direction corresponding to the superconducting gap node, the imaginary part of the self-energy has a linear temperature dependence, independent of binding energy, for small energies, and a linear energy dependence, independent of temperature, for large binding energies [5]. This behavior is embodied in the marginal Fermi liquid model, which is characterized by a lack of quasiparticles at the Fermi energy [6]. Such behavior, found at temperatures above and below the superconducting transition temperature, is quantum critical in character [5]. The measured temperature dependence of the self-energy and related momentum spread in photoemission is reminiscent of the temperature dependence of the resistivity; linear in T with negligible zero-temperature intersect [7]. As such, it is clearly of interest to determine over what fraction of the Fermi surface the linearity of the momentum spread holds. In the present paper we find that it exists over most of the Fermi surface ($\sim$70%) in the normal state, with a slope that is approximately constant for that portion of the Fermi surface. However, as one moves away from the nodal point, there is an increase in the temperature-independent offset. Only in the immediate vicinity of the $(\pi, 0)$ point, the momentum widths appear to level off, with no temperature dependence. These observations suggest that scattering rates for the in-plane transport [7] are dominated by the behavior measured in the nodal region, and are consistent with models in which the c-axis transport is dominated by physics from $(\pi, 0)$ region [8–10]. In the superconducting state, for points close to the nodal line, the widths continue their linear temperature dependence smoothly from the normal state. Further away from this nodal line, the scattering rates become temperature independent in the superconducting state.

The experimental studies reported in this paper were carried out on a Scienta electron spectrometer [11]. In this instrument, the spectral response may be measured as a function of angle and energy simultaneously. The instrument has an angular resolution of $\pm 0.1°$ or better and, in the present studies, an energy resolution of the order of 10 meV. Photons were provided either by a resonance lamp or by a normal incidence monochromator based at the National Synchrotron Light Source. In the photon energy range used, 15–21.22 eV, the momentum resolution is of the order of 0.005 $Å^{-1}$. Samples of optimally doped ($T_c = 91$ K) $Bi_2Sr_2CaCu_2O_{8+\delta}$, produced by the floating zone method [12], were mounted on a liquid He cryostat and cleaved *in situ* in the UHV chamber with base pressure 3×10^{-11} mbar. During the recording of each spectrum, the temperature was measured using a silicon sensor mounted close to the sample. The self-energy may be determined either from energy distribution curves (EDC) or from momentum distribution curves (MDC). The EDC represents a measure of the intensity as a function of binding energy at constant momentum and the MDC represents a measure of the intensity as a function of momentum at constant binding energy.

In Fig. 1(a) we show the Fermi surface determined in the superconducting state. This Fermi surface is obtained directly by measuring the peak positions in MDCs. We note that the area enclosed by this Fermi surface is consistent

 0031-9007/00/85(4)/828(4)$15.00

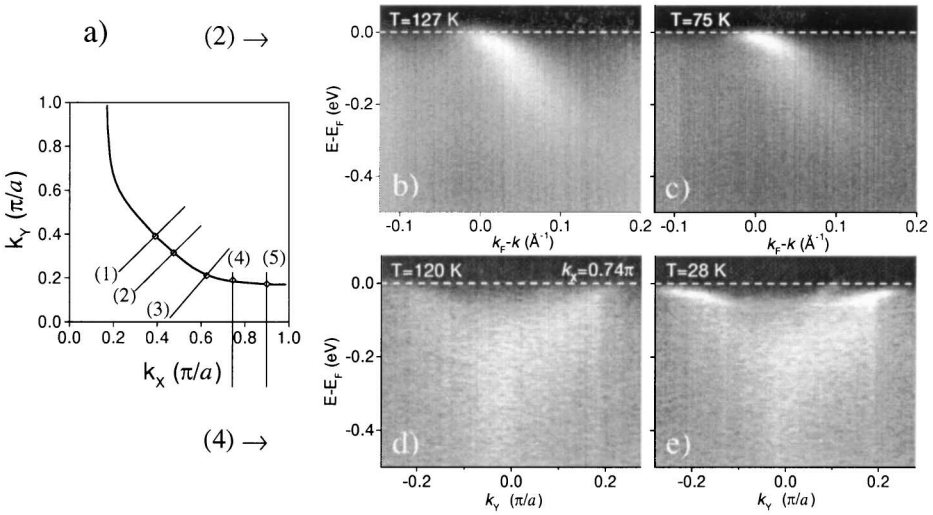

FIG. 1. (a) Fermi surface of the optimally doped Bi2212, measured in the superconducting state. Indicated are the lines (1) to (5) on which the temperature dependence is measured. Typical spectra are shown for line (2) in the normal (b) and superconducting state (c), as well as for line (4), in the normal (d) and superconducting state (e).

with the hole concentration in this optimally doped material. In the rest of the figure, we show representative spectra for line (2) in the normal state (b) and the superconducting state (c) and the same for line (4), closer to the $(\pi, 0)$ region in panels (d) and (e). These spectra represent the measured photoemission intensities as a function of binding energy and parallel momentum. On line (2) the normal state shows a reasonably well-defined dispersing band in the normal state, sharpening as one moves into the superconducting state. On line (4) the normal state is less well defined, but the superconducting state is characterized by a sharp peak appearing close to the Fermi level. It should be noted that this peak actually shows considerable dispersion, as is evident in panel (e).

In Fig. 2 we show in the left panel EDCs for temperatures above and below the transition temperature, for three points on the Fermi surface indicated in Fig. 1(a). In the normal state, peaks become progressively more ill defined as we move closer to the $(\pi, 0)$ region. However, the transition to the superconducting state is marked by the appearance of a sharp peak in the spectra. The anisotropy of the superconducting gap can clearly be seen with the largest gap in the vicinity of the $(\pi, 0)$ point, as found in earlier studies [2]. In the right panel of the figure, we show MDCs measured at the corresponding lines. The measurements in the normal state are recorded at the Fermi energy ($\omega = 0$). Below T_c we show two measurements, the intensity recorded at $\omega = 0$, and the intensity recorded at the leading edge, $\omega = -|\Delta(\mathbf{k}_F)|$. It is obvious that in MDCs, well-defined peaks exist in the normal state even in the vicinity of the $(\pi, 0)$ point. For this reason, we focus on MDCs in our analysis of temperature dependence of the spectral width.

In Fig. 3, we show the measured momentum widths as a function of temperature, for different points around the Fermi surface [13]. Measurements are made at the Fermi level in the normal state and at the leading edge in the superconducting state. The temperature dependence in the normal state is linear for most of the Fermi surface from the (π, π) direction out towards the $(\pi, 0)$ point. Furthermore, the temperature slope is similar over most of the same region. However, there is a marked increase in the temperature-independent offset as one moves away from the node. Indeed we may describe the temperature dependence of momentum widths as $\Delta k(\mathbf{k}_F, T) = a(\mathbf{k}_F) + bT$, where $a(\mathbf{k}_F)$ is momentum dependent but temperature independent and b, the slope, is approximately momentum independent. In the immediate vicinity of the $(\pi, 0)$ point, it is possible that the slope has leveled off, leaving no temperature dependence in the normal state. The measurements from this latter region may be influenced by the strong k-dependence of matrix elements near the $(\pi, 0)$ point, and additionally complicated by the presence of the umklapps (see bottom right panel of Fig. 2, for example).

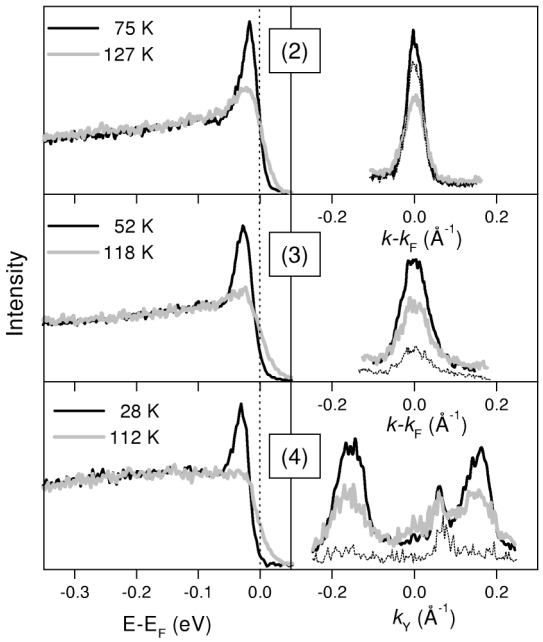

FIG. 2. EDCs (left panel) and MDCs (right panel) for lines (2), (3), and (4) from Fig. 1(a), in the normal (gray lines) and superconducting state (black lines). In the superconducting state, the MDCs are measured at the Fermi level (dashed lines) and at the leading edge (solid lines).

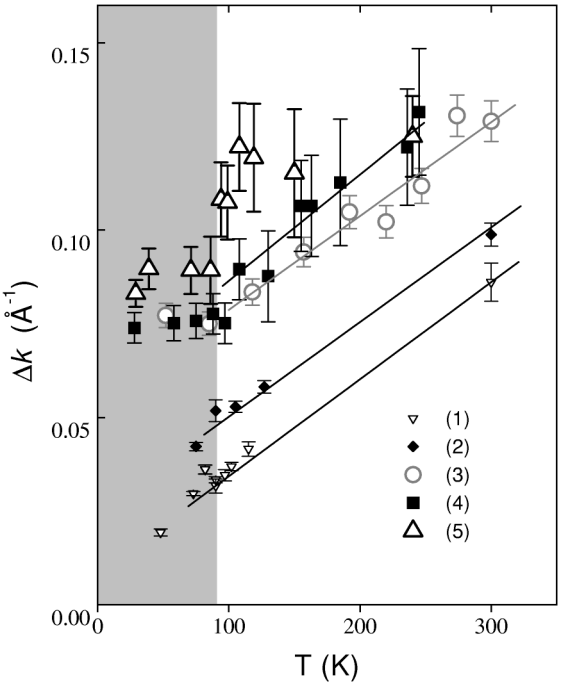

FIG. 3. Momentum widths (components perpendicular to the Fermi surface) as a function of temperature for different positions on the Fermi surface, obtained by fitting the MDCs with Lorentzian line shapes. Widths are measured at the Fermi level and at the leading edge, in the normal and in the superconducting (gray region) state, respectively.

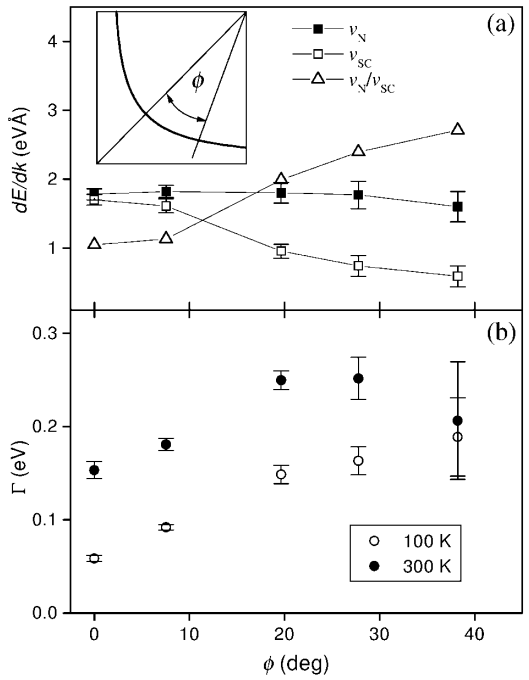

FIG. 4. (a) Fermi velocities (components perpendicular to the Fermi surface) in the normal (solid squares) and superconducting (open squares) state as a function of the angle ϕ, defined in the inset (see text for details). The ratios between the normal state and superconducting state velocities are also shown (open triangles). (b) Normal state scattering rates as a function of ϕ, obtained by multiplying momentum widths from Fig. 3 with normal state velocities.

Therefore, uncertainties are largest in this region. In the superconducting state, the momentum widths appear to saturate as one moves away from the nodal line. This is consistent with the emergence of a sharp peak in the EDCs, which has a temperature-independent width [14].

The product of the momentum widths and the Fermi velocities provides the scattering rates or inverse lifetimes. In Fig. 4(a), we show the measured velocities as a function of position around the Fermi surface. Velocities were obtained from dispersions deduced from MDCs. The low energy part in such a dispersion (-50 meV $< \omega < 0$, for the normal state, and -50 meV $< \omega < -|\Delta(\mathbf{k}_F)|$, for the superconducting state) is then fitted by a straight line, with the slope representing the velocity. The velocity is shown both for the normal state, ν_N, where it appears to be nearly constant over a large fraction of the Fermi surface, and for the superconducting state, ν_{SC} [15]. The ratio of the velocities ν_N/ν_{SC} is also shown. Note that due to the change in velocity, the scattering rates are significantly reduced below T_c for points away from the node. Finally, in Fig. 4(b) we show the single-particle scattering rates at different points on the Fermi surface for two temperatures, 100 and 300 K. These scattering rates are obtained by multiplying the momentum widths in Fig. 3 by the normal-state velocities indicated in Fig. 4(a).

Now we focus on different aspects of the results presented here for the normal state. From the temperature and $\mathbf{k}_F$ dependence of the single-particle scattering rate (for $\omega = 0$), it is possible to calculate the conductivity in the normal state. In a simple Drude-type model, the conductivity is proportional to the integral of $k_F l$ over the Fermi surface, where k_F is the Fermi wave vector and $l = 1/\Delta k$ is the mean free path. However, the observation in Fig. 3 that Δk has a negligible zero-temperature offset only along the node $a(\mathbf{k}_F) \approx 0$, shows that a simple integration would give an incorrect result for resistivity, the latter acquiring a significant T-independent term. This means that either the nodal excitations play a special role in the normal state transport, or single-particle scattering rates differ significantly from transport rates. That the normal state transport might be dominated by the behavior found in the nodal region, is not unreasonable if one considers the underlying antiferromagnetic structure of these materials. Along the diagonal direction, the spins on neighboring copper sites are ferromagnetically aligned. Along the copper oxygen bond direction transport will be frustrated by the antiferromagnetic alignment of the spins on neighboring copper sites. However, it is also true that transport discriminates scattering events, emphasizing large momentum transfers (small-angle events do not degrade measured currents). For example, recent thermal transport measurements on YBCO have indicated a sharp increase in the mean free path below T_c [16], a behavior different from that found in ARPES for nodal excitations [5]. When the system enters the superconducting state, the phase space for large momentum (angle) transfers collapses and the nodal

excitations decay only through the small-angle events. Evidently, the scattering rates measured in thermal transport will be affected by the transition much more than the single-particle scattering rates measured in ARPES.

Recently, Abrahams and Varma have suggested that the temperature- and energy-independent term $a(\mathbf{k}_F)$ represents the scattering on static impurities, placed between the CuO_2 planes [17]. Such impurities would indeed give rise to small-angle scattering, contributing only to single-particle scattering rates and producing a negligible effect on the resistivity. The strong momentum dependence of $a(\mathbf{k}_F)$ is then explained by a variation in the density of states which is available for small-angle scattering at the corresponding momentum. In this picture, the only term relevant for the normal state transport is the temperature- and energy-dependent, but momentum-independent marginal Fermi liquid self-energy.

In a different approach to explain the linearity in the measured resistivity, Ioffe and Millis [9] have suggested that the single-particle scattering rates should contain a temperature-independent term with $\sin^2(2\phi)$ dependence, where ϕ is defined as in Fig. 4. However, the present data show approximately linear dependence for small ϕ and more importantly, the linear temperature and energy dependence for the nodal direction [5], as opposed to the quadratic dependence of a Fermi liquid, used in their model.

Consideration of the anisotropy of the c-axis hopping integral has lead several authors to propose that the anomalous c-axis transport in these materials is dominated by scattering rates in the vicinity of the $(\pi, 0)$ point [8–10]. The c-axis resistivity for the optimally doped material is approximately constant over the range from 250 down to 150 K, at which point there is an increase before a rapid drop to zero at T_c [18]. The experimental points in Fig. 3 corresponding to the $(\pi, 0)$ region are consistent with this temperature dependence. Any integration over the Fermi surface, even if weighted by matrix elements, would give rise to a linear term in the c-axis resistivity. Our preliminary results on highly overdoped samples ($T_c \sim 50$ K), show that the correspondence between the behavior in the $(\pi, 0)$ region and c-axis resistivity may indeed be generic and exist through a wide range of doping levels [19]. In the latter case, we have detected greater temperature dependence in the $(\pi, 0)$ region than in optimally doped samples, in agreement with the c-axis resistivity becoming more metallic in the overdoped regime. This correspondence is a strong indication that the anomalous c-axis transport may be a consequence of the in-plane physics in the $(\pi, 0)$ region.

In summary, the present study has shown that in the normal state, the linear temperature dependence observed for the imaginary part of the self-energy extends over at least 70% of the Fermi surface. The scattering rates are highly anisotropic with a minimum along the nodal direction.

The authors would like to acknowledge useful discussions with V. J. Emery, B. O. Wells, C. M. Varma, E. Abrahams, and G. Sawatzky. The work was supported in part by the Department of Energy under Contract No. DE-AC02-98CH10886, and in part by the New Energy and Industrial Technology Development Organization (NEDO).

[1] J. C. Campuzano *et al.,* Phys. Rev. Lett. **64**, 2308 (1990); D. S. Dessau *et al.,* Phys. Rev. Lett. **71**, 2781 (1993); P. Aebi *et al.,* Phys. Rev. Lett. **72**, 2757 (1994).
[2] B. O. Wells *et al.,* Phys. Rev. B **46**, 11 830 (1992); Z.-X. Shen *et al.,* Phys. Rev. Lett. **70**, 1553 (1993); H. Ding *et al.,* Phys. Rev. B **54**, R9678 (1996).
[3] A. G. Loeser *et al.,* Science **273**, 325 (1996).
[4] H. Ding *et al.,* Nature (London) **382**, 51 (1996).
[5] T. Valla *et al.,* Science **285**, 2110 (1999).
[6] C. M. Varma *et al.,* Phys. Rev. Lett. **63**, 1936 (1989).
[7] M. Gurvitch and A. T. Fiory, Phys. Rev. Lett. **59**, 1337 (1987).
[8] S. Chakravarty, A. Sudbo, P. W. Anderson, and S. Strong, Science **261**, 337 (1993); O. K. Andersen *et al.,* J. Phys. Chem. Solids **56**, 1573 (1995).
[9] L. B. Ioffe and A. J. Millis, Science **285**, 1241 (1999); cond.mat/9908366.
[10] D. van der Marel, Phys. Rev. B **60**, 6631 (1999).
[11] P. D. Johnson *et al.,* in Proceedings of the 11th Annual Synchrotron Radiation Conference (AIP Press, New York, to be published).
[12] G. D. Gu, K. Takamuku, N. Koshizuka, and S. Tanaka, J. Cryst. Growth **130**, 325 (1990).
[13] The lines (2) to (5) are not perpendicular to the Fermi surface. However, since the discrepancy is small, and since $\Delta k \ll k_F$, it is straightforward to extract perpendicular components of momentum widths and velocities [shown in Fig. 3 and Fig. 4(a)].
[14] A. V. Fedorov *et al.,* Phys. Rev. Lett. **82**, 2179 (1999).
[15] If the self-energy is a strongly varying function of ω, with significant constant term in its imaginary part, the position of the "sharp" peak in EDCs (usually the spectrum has a characteristic "two-peak structure") does not represent the one-particle dispersion any more. On the other hand, if the self-energy depends only weakly on $\mathbf{k}$, the MDCs have much simpler line shape, and the peak position will approximately follow the one-particle dispersion. Therefore, velocities deduced from MDCs are more accurate than those extracted from EDCs. However, the finite instrumental resolution will affect such measurements progressively more as velocities decrease. In the superconducting state, $v_{SC} \rightarrow 0$ for $\omega = -|\Delta(\mathbf{k}_F)|$ (particle-hole mixing), and our velocities become approximations, representing mean values over the measured energy interval. This is valid within the "quasiparticle" picture. However, if the injected hole decays into more fundamental excitations, the photoemission spectrum loses the "quasiparticle pole" and both the EDCs and MDCs represent a broad many-particle continuum.
[16] N. P. Ong, K. Krishana, Y. Zhang, and Z. A. Xu, cond-mat/9904160.
[17] E. Abrahams and C. M. Varma, Proc. Natl. Acad. Sci. U.S.A. **97**, 5714 (2000).
[18] X. H. Chen *et al.,* Phys. Rev. B **58**, 14 219 (1998); T. Motohashi *et al.,* Phys. Rev. B **59**, 14 080 (1999).
[19] Z. Yusof *et al.* (to be published).